ADVANCED OPTICAL MATERIALS
www.advopticalmat.de

Halogen-Hot-Injection Synthesis of Mn-Doped $CsPb(Cl/Br)_3$ Nanocrystals with Blue/Orange Dual-Color Luminescence and High Photoluminescence Quantum Yield

Daqin Chen, Su Zhou, Feifan Tian, Haitao Ke, Naizhong Jiang, Shujin Wang, Yongzhao Peng, and Yue Liu*

Recently, Mn^{2+}-doped $CsPb(Cl/Br)_3$ perovskite nanocrystals (NCs), showing the advantages of dual-color emissions via exciton-to-dopant energy transfer and reduced usage of toxic Pb^{2+} heavy metal ions by nontoxic Mn^{2+} substitution, are widely explored. However, photoluminescence quantum yields (PLQYs) for Mn^{2+}-doped $CsPb(Cl/Br)_3$ NCs still need to be further improved. Here, a halogen-hot-injection strategy is developed to prepare $Mn:CsPb(Cl_{0.6}Br_{0.4})_3$ NCs with the maximal PLQY of 65%. With this method, intense blue narrowband emission from excitonic recombination and orange broadband emission from Mn^{2+} $^4T_1 \rightarrow {}^6A_1$ transition can be simultaneously achieved. The competitive luminescence between perovskite NCs and Mn^{2+} dopants is systematically investigated by controlling the injected halogen types and ratios. As a proof-of-concept experiment, the present Mn^{2+}-doped $CsPb(Cl/Br)_3$ perovskite NCs with highly efficient dual-color emissions are demonstrated to be applicable as color converter in UV-excitable solid-state lighting.

Metal halide perovskite quantum dots (PQDs) or nanocrystals (NCs) have been extensively investigated in recent years. Due to their unique optical properties, such as narrow full width at half maxima (12–42 nm), tunable bandgap energies through 410–700 nm, and high photoluminescence quantum yields (PLQYs, exceeding 90%), PQDs are considered as potential candidates for light-emitting diodes (LEDs), displays, and lasers.[1–11] However, the toxicity of PQDs limit their practical applications. Bivalent manganese (Mn^{2+}) doping was widely studied in semiconductor materials like CdS, ZnS,[12–15] and as identical valance with Pb^{2+} in lead halide perovskite, Mn^{2+} can be introduced into $CsPbX_3$ host by substituting Pb^{2+} to reduce the usage of Pb^{2+} heavy metal ions. Additionally, energy transfer (ET) from perovskite host to Mn^{2+} dopants can result in extra Mn^{2+} red luminescence assigned to d–d transition.[16] Compared to II–VI group semiconductors, PQDs are regarded as appropriate hosts to efficiently sensitize Mn^{2+} emission benefited from their high absorption coefficient, narrow emission width, and long excited-state lifetime.[17] The primary parameter to influence energy transfer and Mn emission intensity is energy difference (ΔE_g) between band-to-band emission of PQD and $^4T_1 \rightarrow {}^6A_1$ transition of Mn^{2+}.[18] When ΔE_g value (0.7–0.9 eV) is appropriate, an intense Mn emission can be obtained; however, decreasing ΔE_g intensifies back transfer (BT) from doped Mn^{2+} centers to the perovskite host, leading to the weakening or even disappearing of Mn^{2+} luminescence.[18–20]

$CsPbCl_3$ PQDs have been reported to be the ideal host for efficiently transferring excitonic energy to Mn^{2+} because of their appropriate bandgap of 3.0 eV.[18] When Cl was gradually replaced by Br, the bandgap of $CsPb(Cl/Br)_3$ PQDs becomes smaller and ET from PQDs to Mn^{2+} is inefficient, leading to weak Mn^{2+} luminescence. As tabulated in Table S1 (Supporting Information), for a classic Cs-hot-injection method using $PbBr_2$ and $MnCl_2$ as the precursors, the as-prepared $Mn:CsPb(Cl/Br)_3$ with excitonic emission at blue region (430–480 nm) has a low PLQY (31%) and Mn^{2+} emission can be barely observed;[17] for a room-temperature supersaturated crystallization method, a high-content $MnCl_2$ precursor is required, causing low PLQY of excitonic emission and concentration quenching of Mn^{2+} luminescence.[21,22] Furthermore, $Mn:CsPb(Cl/Br)_3$ PQDs can also be fabricated by a postsynthetic cation exchange and the bandgap of exciton can be tuned over a wide range, but the maximal PLQY is only 28%.[23] More recently, strong Mn^{2+} emission

Dr. D. Q. Chen, F. F. Tian, H. T. Ke, N. Z. Jiang, S. J. Wang
College of Physics and Energy
Fujian Normal University
Fuzhou 350117, China
E-mail: dqchen@fjnu.edu.cn
Dr. D. Q. Chen, F. F. Tian, H. T. Ke, N. Z. Jiang, S. J. Wang
Fujian Provincial Collaborative Innovation Center for Optoelectronic Semiconductors and Efficient Devices
Xiamen 361005, China
S. Zhou, Y. Z. Peng, Y. Liu
College of Materials & Environmental Engineering
Hangzhou Dianzi University
Hangzhou 310018, China
The ORCID identification number(s) for the author(s) of this article can be found under https://doi.org/10.1002/adom.201901082.

DOI: 10.1002/adom.201901082

in $Mn:Cs(Pb/Zn)(Cl/Br)_3$ perovskite NCs with high Br^- content was realized through the ion exchange reaction occurring between $ZnBr_2$ and preformed $Mn:CsPbCl_3$ NCs.[24] However, this strategy required elaborate control of anion exchange and cation exchange rates. Therefore, exploring a novel strategy to synthesize Mn-doped $CsPb(Cl/Br)_3$ PQDs with blue/orange dual-color emissions and high PLQYs is highly desirable.

Herein, we report the synthesis of Mn-doped $CsPbX_3$ (X = Cl, Br, I) NCs via a one-pot halogen-hot-injection method. Different to the case previously reported, manganese acetate ($Mn(Ac)_2$), lead acetate ($Pb(Ac)_2$), and cesium carbonate (Cs_2CO_3) were dissolved in octadecene (ODE) and oleic acid (OA) first, and then oleylamine–X (OAm–X, X = Cl, Br, I, and their mixture) was swiftly injected into the solution at 250 °C. Selected Mn precursor, $Mn(Ac)_2$ can break the demanding limit of previously reported bond dissociation energy matching between Pb–X and Mn–X. And, the emissive color produced by the combination of exciton recombination and Mn^{2+} radiation can be precisely controlled by feeding ratio of different halogens. Importantly, the PLQYs for the as-prepared $Mn:CsPbCl_3$ and $Mn:CsPb(Cl_{0.6}Br_{0.4})_3$ NCs reach up to 58% and 65%, respectively. As far as we know, the value for Mn-doped $CsPb(Cl/Br)_3$ NCs is the maximal one reported so far. Both strong blue emission of exciton recombination at ≈450 nm and orange broadband emission of Mn^{2+}:$^4T_1 \rightarrow {}^6A_1$ transition at ≈600 nm can be discerned, enabling $Mn:CsPb(Cl/Br)_3$ NCs find promising application as color converter in solid-state lighting.

The detailed halogen-hot-injection procedure is schematically illustrated in **Figure 1**. For a typical $Mn:CsPb(Cl_{0.6}Br_{0.4})_3$ sample, we used $Mn(Ac)_2$, $Pb(Ac)_2$ (0.2 mmol), and cesium carbonate (Cs_2CO_3, 0.1 mmol) as precursors dissolved in ODE (10 mL) and OA (1 mL), then the prepared OAm–Cl and OAm–Br solution (1 mL, 1 mmol) with Cl-to-Br molar feeding ratio of 0.6:0.4 was swiftly injected at 250 °C. In fact, several reaction temperatures have been employed in the present work. With elevation of temperature from 190 to 250 °C, PLQY value of the product gradually increases. However, further increasing temperature will lead to the formation of impurity phase. Therefore, 250 °C is selected as the best temperature to get product with high PLQY. Inductively coupled plasma mass spectrometry (ICP-MS) measurements reveal that 0.8%, 1.7%, 4.5%, and 10.4% Mn^{2+} can be introduced into perovskite hosts with Mn-to-Pb mole feeding ratios of 0.5:1, 1:1, 2:1, and 5:1, respectively. X-ray diffraction (XRD) patterns of the prepared Mn-doped products are well coincident with tetragonal $CsPbCl_3$ phase (PDF#18-0366) and increasing Mn^{2+} doping content induces slightly shift of peaks toward high angle (**Figure 2**a), which is attributed to the substitution of Pb^{2+} by Mn^{2+} with smaller ionic radius.[25] Electron spin-resonance spectroscopy (ESR) spectrum (Figure 2b) demonstrates distinct sextet hyperfine splitting lines, confirming that Mn^{2+} dopants are successfully incorporated into perovskite lattice.[26,27] Transmission electron microscope (TEM) and high-resolution TEM (HRTEM) are provided in Figure 2c,d. The size distribution histogram (Figure S1, Supporting Information) demonstrates that the average size of perovskite NCs are around 19 nm, which is much larger than previous reported,[19,25,28] probably due to high reaction temperature (250 °C). HRTEM of an individual particle and the corresponding fast Fourier transformation (FFT) pattern evidence its high crystallinity and the well-resolved lattice fringes with a typical (110) *d*-spacing of 0.39 nm. High-angle annular dark-field scanning TEM (HAADF-STEM) image (Figure 2e) together with the element mappings (Figure 2f–j) on a single Mn-doped $CsPb(Cl_{0.6}Br_{0.4})_3$ NCs demonstrate the homogeneous distribution of Cs, Pb, Cl, Br, and Mn signals, further verifying the incorporation of Mn^{2+} dopants into perovskite host. Based on energy dispersive X-ray (EDX) spectroscopy of Mn-doped $CsPb(Cl_{0.6}Br_{0.4})_3$ NCs (Figure S2a, Supporting Information), the Mn to Pb mole ratio is evaluated to be about 1:9, being in accordance with the ICP-MS result.

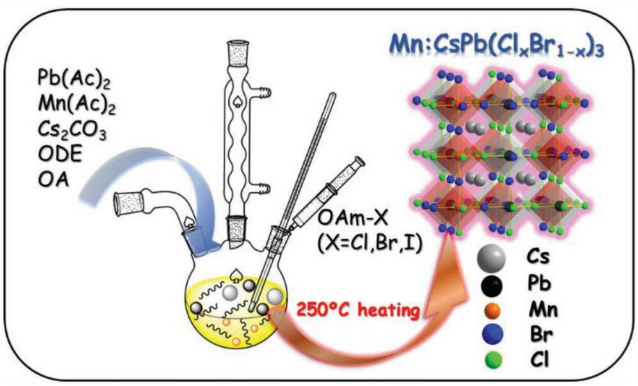

Figure 1. Schematic illustration of the synthesis procedure for the Mn-doped $CsPbX_3$ NCs by a halogen-hot-injection strategy.

Photoluminescence (PL) spectra of $Mn:CsPb(Cl_{0.6}Br_{0.4})_3$ NCs synthesized with different Mn-to-Pb feeding ratios are shown in **Figure 3**a. All the spectra are normalized to exciton emission peak at blue region. Dual emissive peaks can be discerned, where blue emission at around 455 nm is originated from exciton recombination of perovskite host and orange emission is assigned to $^4T_1 \rightarrow {}^6A_1$ transition of Mn^{2+} dopants. A small blueshift from 458 to 450 nm of exciton emission is due to the modification of perovskite bandgap via the substitution of Pb^{2+} by smaller Mn^{2+} ions. This result is in accordance with the corresponding absorption spectra, where the absorption band gradually shifts toward higher energy (Figure 3b). The Mn^{2+} emission relative to exciton one monotonously enhances with increase of Mn-to-Pb feeding ratio, being consistent with previous results of $Mn:CsPbCl_3$ NCs.[25] To further understand the optical properties of $Mn:CsPb(Cl_{0.6}Br_{0.4})_3$ NCs, PLQYs and time-resolved PL behaviors of exciton and Mn^{2+} were measured (Figure 3c,d and Figure S2b (Supporting Information)). For the undoped $CsPb(Cl_{0.6}Br_{0.4})_3$ NCs, only 38% PLQY was obtained in this work, which is lower than near-unity PLQY reported by Pradhan and co-workers.[29] But, a significant increase in PLQY can be achieved upon Mn^{2+} doping, which reaches as high as 65% for 1.7% Mn-doped sample. The high PLQYs are probably ascribed to high reaction temperature and passivation of crystal defect due to excess halogen ions.[30–32] In this method, with fixed Cs-to-Pb ratio of 1:1, post-halogen-injection shows the advantage of facile control halogen content to tune halogen-to-Pb ratio. Herein, high halogen-to-Pb ratio is used to produce halogen-rich reaction environment, which is beneficial to reduce halogen vacancies on the surface of NCs. Additionally, higher reaction temperature (250 °C) can improve

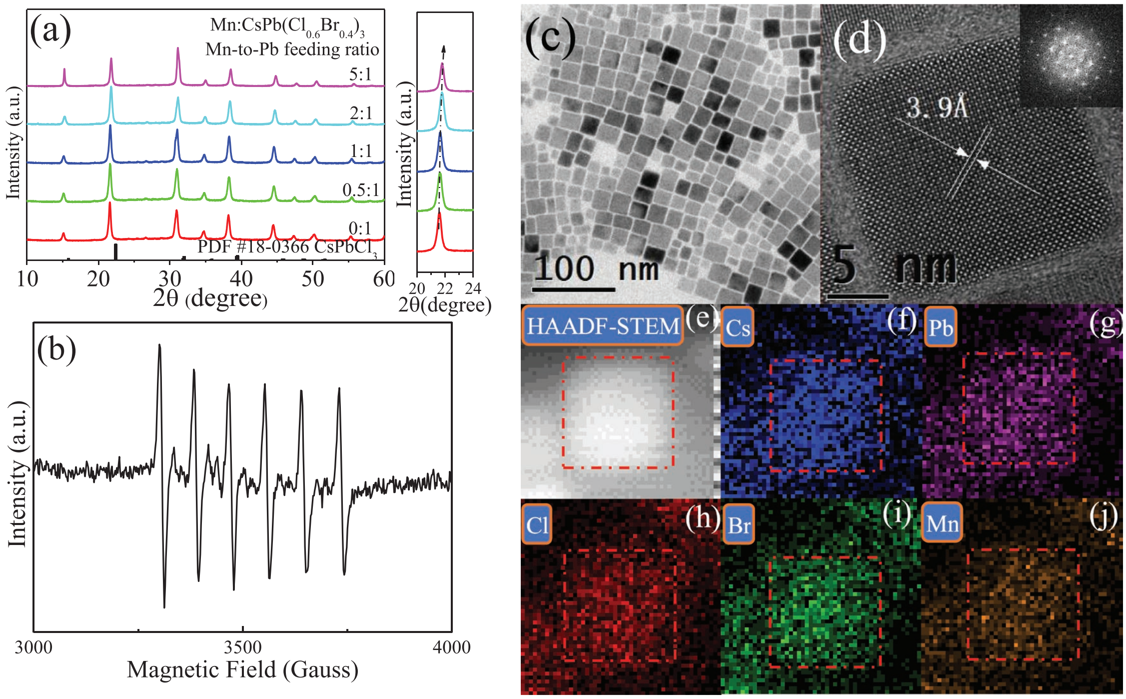

Figure 2. a) XRD patterns of typical Mn-doped $CsPb(Cl_{0.6}Br_{0.4})_3$ NCs prepared with various Mn-to-Pb feeding ratios. Bars represent standard diffraction data of tetragonal $CsPbCl_3$ phase (PDF # 18-0366). b) ESR spectrum of Mn:$CsPb(Cl_{0.6}Br_{0.4})_3$ measured at room temperature. c) TEM image of Mn:$CsPb(Cl_{0.6}Br_{0.4})_3$. d) HRTEM image of an individual Mn:$CsPb(Cl_{0.6}Br_{0.4})_3$ particle and its FFT pattern. e) HAADF-STEM image of a single Mn:$CsPb(Cl_{0.6}Br_{0.4})_3$ particle and f–j) the corresponding EDX element mapping of Cs, Pb, Cl, Br, and Mn.

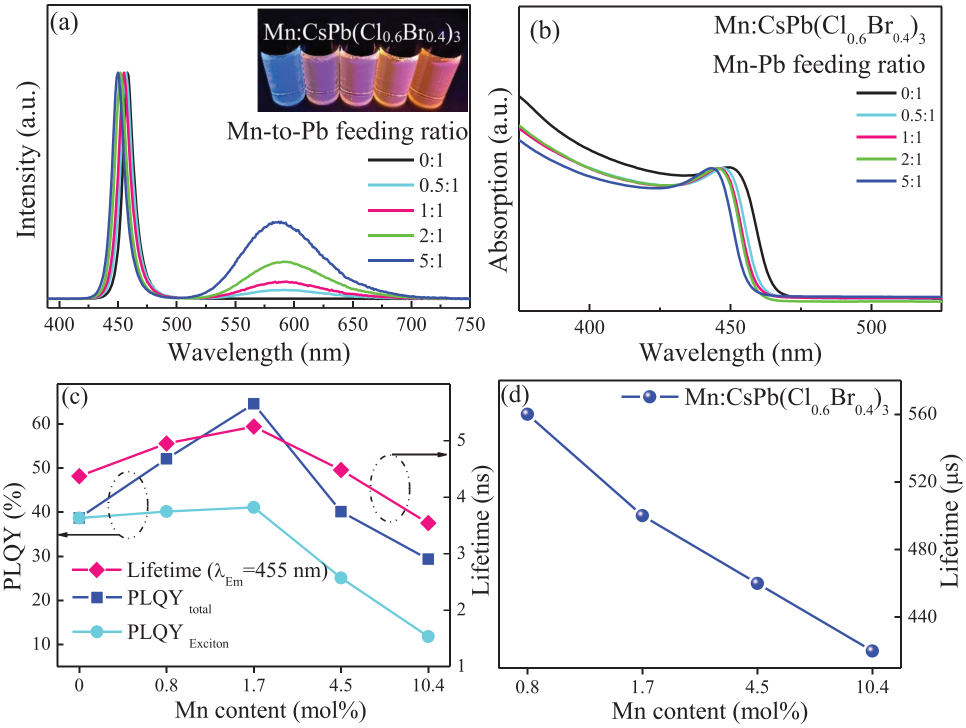

Figure 3. a) PL spectra of Mn:$CsPb(Cl_{0.6}Br_{0.4})_3$ NCs with different Mn^{2+} doping contents. Insets are luminescent photographs of Mn:$CsPb(Cl_{0.6}Br_{0.4})_3$ NCs in solution under irradiation of 365 nm UV lamp. b) Absorption spectra for the corresponding samples. c) PLQYs of excitonic emission, total emissions, and decay lifetime of excitonic emission versus Mn doping content. d) Mn-content-dependent decay lifetime by monitoring Mn^{2+}:$^4T_1 \rightarrow {}^6A_1$ transition.

crystallinity of perovskite NCs and reduce their internal defects. All these advantages are helpful to enhance PLQY. The lifetime in the nanosecond scale for the excitonic emission was detected by 375 nm pulse laser, which increases from 4.37 to 5.25 ns for low Mn doping and decreases to 3.54 ns with heavy Mn doping. The shortened lifetime of excitonic emission under heavy doping condition is ascribed to the intensified energy transfer from perovskite host to Mn^{2+} activators.[23,33] The Mn^{2+} lifetime in the millisecond scale was demonstrated in Figure 3d. The monotonous decrease of Mn^{2+} lifetime is attributed to concentration quenching effect of Mn^{2+} luminescence, further confirming the increase of Mn^{2+} doping content in perovskite host. Similarly, Mn-doped $CsPbCl_3$ NCs can be synthesized by this halogen-hot-injection method (Figure S3, Supporting Information). As shown in Figure S4a (Supporting Information), Mn^{2+} emission intensity relative to excitonic one gradually enhances with increase of Mn-to-Pb feeding ratio, and blueshift of excitonic emission in the violet region can be observed, indicating the successful preparation of Mn-doped $CsPbCl_3$ product. The maximal incorporating content of Mn^{2+} dopants in $CsPbCl_3$ is determined to be 25% (ICP-MS result) with Mn-to-Pb feeding ratio of 5:1 and ESR spectrum clearly distinct hyperfine splitting lines of Mn^{2+} in $CsPbCl_3$ crystalline lattice (Figure S5, Supporting Information). Notably, the six distinct ESR peaks for Mn-doped $CsPbCl_3$ product tend to merge together to give rise to a single strong broad peak, which is attributed to high Mn doping content in $CsPbCl_3$ lattice.[26] The maximal PLQY of Mn:$CsPbCl_3$ NCs reaches 58% with Mn-to-Pb feeding ratio of 1:1 (Figure S4b, Supporting Information). Similar to the previous report,[25,34,35] the lifetimes of both excitonic recombination and Mn^{2+} d–d transition decrease with increase of Mn^{2+} doping content (Figure S4c, Supporting Information).

In a further experiment, Mn-doped $CsPb(Cl_xBr_{1-x})_3$ NCs with variation of Cl-to-Br ratios were synthesized. XRD patterns evidence that Mn:$CsPbCl_3$ NCs are of tetragonal phase (PDF #18-0366), and change to monoclinic $CsPbBr_3$ phase (PDF#18-0346) with increase of Br-to-Cl ratio (Figure S6, Supporting Information), and the corresponding diffraction peaks gradually shift toward low-angle direction. PL spectra (**Figure 4**a) show tunable excitonic emission from 401 to 518 nm by changing molar feeding ratio of OAm–Cl/OAm–Br, verifying the narrowed bandgap of perovskite NCs and the successful formation of $CsPb(Cl/Br)_3$ NCs with variable Cl-to-Br ratios. This is further confirmed by the gradual redshift of excitonic absorption for the corresponding products (Figure S7, Supporting Information). For Mn^{2+} emission, a slight blueshift from 602 to 587 nm with increase of Br-to-Cl ratio is clearly observed (Figure 4a and Figure S8 (Supporting Information)), which is ascribed to the alteration of Mn^{2+} ligand field in perovskite hosts.[36] In MnX_6^{4-} octahedron, Mn^{2+} ions are surrounded by six halogen ions,[35,37] the substitution of Cl by Br with larger ionic radius will cause lattice expansion and lead to weaker crystal field. As revealed in Tanabe–Sugano diagram (Figure S9, Supporting Information), Mn^{2+} $^4T_1$ excited state is highly sensitive to ligand field and will be elevated to higher energy in weaker crystal filed environment, resulting in the blueshift of Mn^{2+} luminescence accompanied with the gradual replacement Cl by Br in host. Decay lifetime of exciton recombination increases from 0.47 ns for Mn:$CsPbCl_3$ NCs to 6.19 ns for Mn:$CsPbBr_3$ NCs (Figure 4b), which is due to increase of bandgap of perovskite. Mn^{2+} decay lifetime significantly decreases from 1.29 ms in $CsPbCl_3$ host to 0.31 ms in $CsPb(Cl_{0.5}Br_{0.5})_3$ (Figure 4b), being attributed to the alteration of ligand-field of Mn^{2+} dopants from $[MnCl_6]$ octahedron into $[Mn(Cl/Br)_6]$ one.

To investigate the influence of bandgap energy of perovskite host on energy transfer of exciton to dopants, the Mn-to-exciton emission peak intensity ratio (EPIR) versus ΔE_g (energy difference between exciton recombination and Mn^{2+} $^4T_1 \rightarrow {}^6A_1$) is determined and plotted in Figure 4c. The maximal EPIR is 7.3 for the Mn:$CsPbCl_3$ sample ($\Delta E_g = 0.9$), and its value reduces to 2.1 for the Mn:$CsPb(Cl_{0.9}Br_{0.1})_3$ sample ($\Delta E_g = 0.8$). With Cl^- ions further substituted by Br^- ones, the EPIR decreases obviously, and almost no Mn^{2+} emission is observed when ΔE_g reaches 0.5 eV. Energy band and energy state diagrams for the present Mn-doped $CsPb(Cl/Br)_3$ NCs are schematically illustrated in Figure 4d, demonstrating dual-color emissions from band-edge exciton recombination of perovskite NCs and $^4T_1 \rightarrow {}^6A_1$ radiative transition of Mn^{2+} as well as the pathway of energy transfer from perovskite host to Mn^{2+} and back transfer from Mn^{2+} to perovskite. Compared to exciton recombination in nanosecond scale, Mn^{2+} $^4T_1$ excited state has a long decay lifetime, i.e., radiative transition occurs in millisecond scale. In this case, BT process will be dominant and overcome ET one in the low ΔE_g condition. The excitons tend to recombine between conductive band and valence band of perovskite rather than transfer to Mn^{2+} dopants, leading to the disappearance of Mn^{2+} luminescence with increase of Br content (decrease of ΔE_g). Back energy transfer requires thermal activation when bandgap of perovskite host cannot completely match with Mn^{2+} energy states, indicating that it is possible to observe Mn^{2+} luminescence in perovskite hosts with high Br content at a low temperature. To verify this, PL spectra for the Mn:$CsPb(Cl_xBr_{1-x})_3$ (x = 0.3,0.2, 0.1, and 0) samples are recorded at 77 K, as shown in Figure 4e–i. Indeed, Mn^{2+} broadband luminescence for all these high-content Br or even pure Br–contained perovskite samples can be easily observed.

Furthermore, we also synthesized Mn-doped $CsPbI_3$ NCs with the halogen-hot-injection method. ICP-MS result indicted that about 1.5 mol% Pb^{2+} ions in $CsPbI_3$ host was substituted by Mn^{2+} dopants. PL spectra of Mn:$CsPbI_3$ NCs prepared with various Mn-to-Pb feeding ratios are provided in Figure S10a (Supporting Information). No Mn^{2+} emission was detected for all these samples due to energy mismatch between exciton recombination (1.7 eV) and Mn^{2+} $^4T_1 \rightarrow {}^6A_1$ transition (2.1 eV).[18,38] Interestingly, the decay lifetime of $CsPbI_3$ NCs is found to increase from 20.1 to 71.8 ns (Figure S10b,c, Supporting Information) and the PLQY value can be effectively improved from 36% to 60% upon Mn^{2+} doping (Figure S10c, Supporting Information). Similar to the cases of Mn-doped $CsPb(Cl/Br)_3$, the PL peak position of $CsPbI_3$ NCs shows a tendency of blueshift from 690 to 685 nm with increase of Mn-to-Pb feeding ratio (Figure S10c, Supporting Information).

Finally, we explored the promising application of the as-prepared Mn:$CsPb(Cl_{0.6}Br_{0.4})_3$ NCs with highly efficient dual-color emissions as color converter in solid-state lighting. As a proof-of-concept experiment, LED devices were constructed by coupling blue/orange Mn:$CsPb(Cl_xBr_{1-x})_3$ and green $CsPbBr_3$ emitting layers with 365 nm UV chip (**Figure 5**a). To avoid

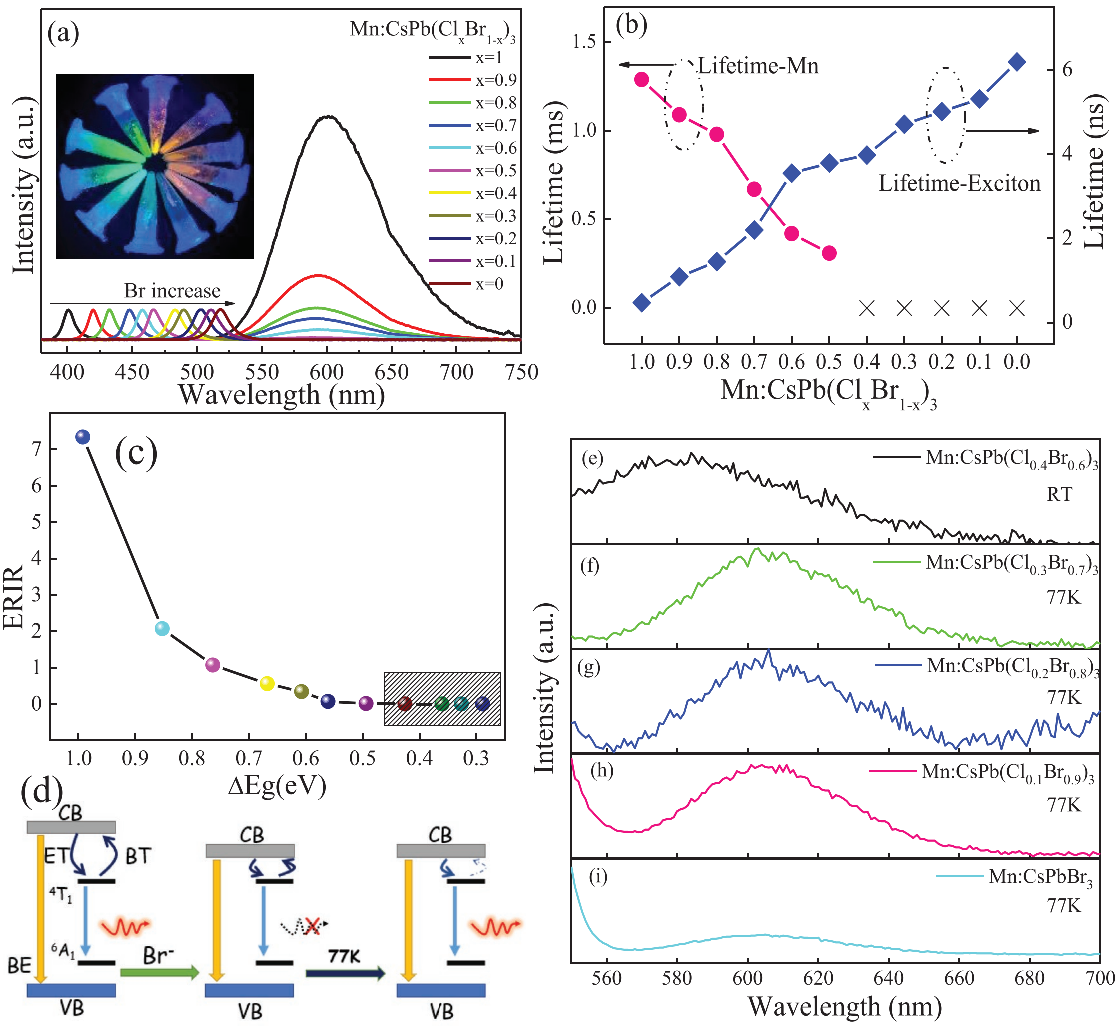

Figure 4. a) PL spectra of Mn:CsPb(Cl$_x$Br$_{1-x}$)$_3$ NCs with increase of Br content (for exciton emission: x = 1–0 from left to right). b) Decay lifetime of Mn (left) and perovskite host (right) in the Mn:CsPb(Cl$_x$Br$_{1-x}$)$_3$ NCs versus x value. c) Mn-to-exciton emission peak intensity ratio (EPIR) versus ΔE_g. d) Schematic illustration of energy transfer (ET) and back transfer (BT) between perovskite host and Mn dopants at room temperature and low temperature (77 K). Enlarged PL spectrum for e) Mn:CsPb(Cl$_{0.4}$Br$_{0.6}$)$_3$ recorded at room temperature and f–i) Mn:CsPb(Cl$_x$Br$_{1-x}$)$_3$ (x = 0.3, 0.2, 0.1, 0) recorded at 77 K to highlight the emerging of Mn emission.

detrimental anion exchange between Mn:CsPb(Cl$_x$Br$_{1-x}$)$_3$ and $CsPbBr_3$, the respective perovskite NCs were spin-coated on the glass slices, respectively. Electroluminescence (EL) spectra show a blue emission band assigned to CsPb(Cl$_{0.6}$Br$_{0.4}$)$_3$ NCs, a green emission band originated from $CsPbBr_3$ NCs, and a broad orange emission band contributed to Mn^{2+} dopants (Figure 5b,c). Notably, the emission band at 365 nm comes from GaN UV chips. Furthermore, driving current dependent EL spectra show that both blue and orange emissions from the Mn:CsPb(Cl$_{0.6}$Br$_{0.4}$) NC layer gradually enhance as the forward current increases from 50 to 300 mA (Figure S11, Supporting Information), confirming that the dual-color emitting layer exhibits no obvious saturation effect toward the incident UV excitation light. The appropriate adjustment of the NC ratios between blue/orange dual-emitting layer and green layer can produce intense white-light luminescence for the constructed solid-state-lighting device with correlated color temperature of 4000 K, color rendering index of 85, luminous efficiency (LE) of 22 lm W^{-1}, and color coordinates of (0.360, 0.354) (Figure 5d,e). These results confirm that the present dual-emitting Mn-doped CsPb(Cl/Br)$_3$ NCs prepared by a halogen-hot-injection method are suitable as a color converter in the phosphor-converted lighting device. Compared to the previously reported values,[24,36] the optoelectronic performance for the fabricated white light-emitting device, especially LE, should be further improved by optimizing device structure and stability of multi-color emitting perovskite components.

In summary, we have developed a novel colloidal synthesis for the Mn^{2+}-doped $CsPbX_3$ (X = Cl, Br, I) perovskite NCs with high PLQYs via a halogen-hot-injection method, which can alleviate the high demand on Mn^{2+} doping precursor (only $MnCl_2$) and enable multicolor tunable emissions by modifying the injected halogen types and ratios. Specifically, intense blue emission of CsPb(Cl$_{0.6}$Br$_{0.4}$)$_3$ exciton recombination and orange emission of Mn^{2+} dopants were simultaneously detected in the Mn-doped CsPb(Cl$_{0.6}$Br$_{0.4}$)$_3$ NCs, leading to the highest

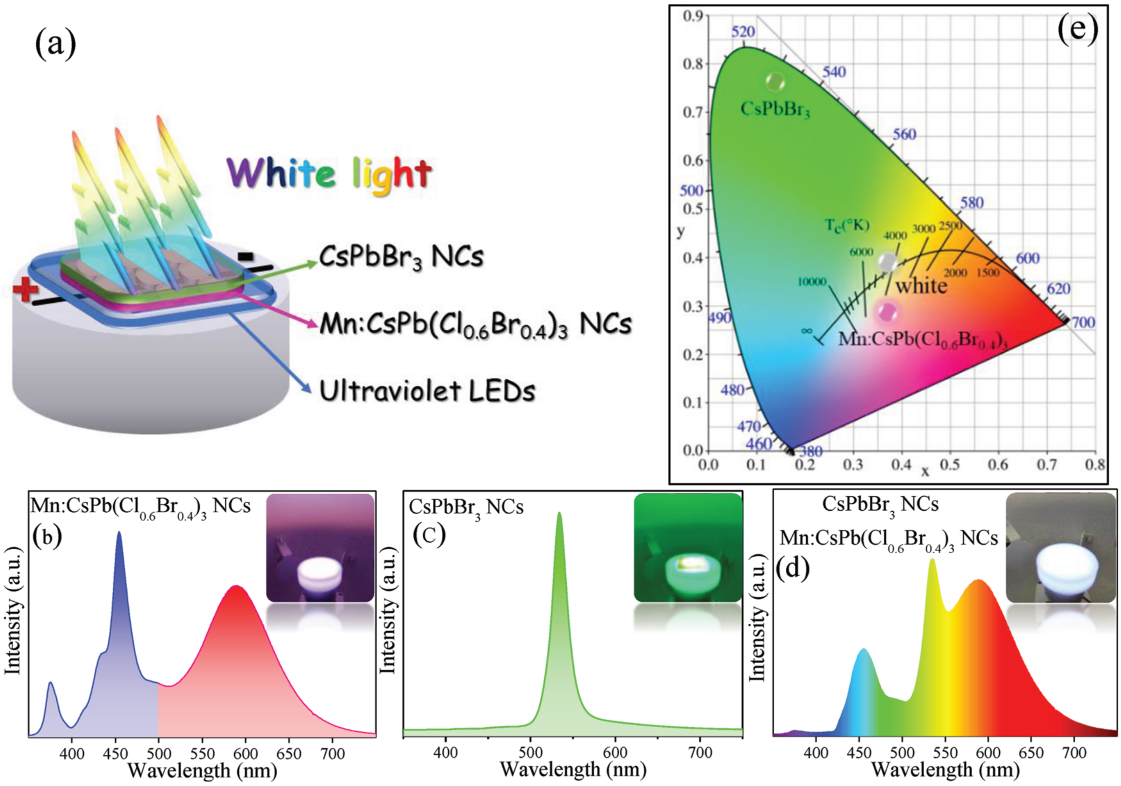

Figure 5. a) Schematic illustration of a prototype LED device by coupling $Mn:CsPb(Cl_{0.6}Br_{0.4})_3$ layer, $CsPbBr_3$ layer, and 365 nm UV chip. EL spectra of devices: b) coupling UV chip with $Mn:CsPb(Cl_{0.6}Br_{0.4})_3$ layer, c) coupling UV chip with $CsPbBr_3$ layer, and d) coupling UV chip with these two emitting layers. Insets are the corresponding luminescent devices under operation. e) CIE chromaticity coordinates for the corresponding devices.

PLQY of 65%. The emission intensity ratio of exciton to Mn^{2+} was highly correlated to energy difference between bandgap of perovskite hosts (3.0–2.4 eV) and Mn^{2+} d–d transition (2.1 eV). With increase of Br content, Mn emission relative to exciton recombination gradually weakened, probably attributing to back energy transfer from dopants-to-hosts via thermal activation. Finally, a prototype all-perovskite LED device was constructed by employing blue/orange dual-emitting $Mn:CsPb(Cl/Br)_3$ NCs and green-emitting $CsPbBr_3$ NCs as color converters, yielding bright white-light luminescence with excellent optoelectronic performance. It is believed that the present work will provide an effective route to easily synthesize Mn-doped perovskite NCs with improved optical properties and even fabricate other low-Pb or Pb-free perovskite materials.

Experimental Section

Materials: ODE (Aladdin, 90%), OA (Aldrich, 90%), OAm (Aladdin, 80–90%), manganese acetate ($Mn(Ac)_2·4H_2O$, Macklin, 99%), lead acetate ($Pb(Ac)_2·3H_2O$, Macklin, 99%), Cs_2CO_3 (Macklin, 99%), HCl (37%, Sinopharm Chemical Reagent Co., Ltd.), HBr (48%, Macklin), HI (48%, Macklin), hexane (Aladdin, 99%), toluene (99% Sinopharm Chemical Reagent Co. Ltd.). All chemicals were directly used without further purification.

Preparation of OAm–X: In a typical preparation of OAm–Cl, OAm (10 mL) and HCl (1 mL) were loaded into a 25 mL three-neck flask, and the mixture was heated to 120 °C for at least 1 h to remove water, then the temperature was raised to 150 °C for 30 min and the mixture was cooled down to room temperature. The reaction was protected by N_2 gas. For OAm–Br and OAm–I, HCl was replaced by HBr and HI, respectively, and other reaction conditions were not altered. Notably, the content of halogen ions in the solution was ≈1 mmol mL^{-1}.

Preparation of $CsPbX_3$ and $Mn:CsPbX_3$ (X = Cl, Br, I) NCs: Taking $CsPb(Cl_{0.6}Br_{0.4})_3$ and Mn-to-Pb molar feeding ratio of 1:1 as a typical example, the synthesizing process was described as follows. $Pb(Ac)_2$ (0.2 mmol), $Mn(Ac)_2$ (0.2 mmol), and Cs_2CO_3 (0.1 mmol) were loaded into a three-neck flask, then ODE (10 mL), OA (1 mL) were loaded, the mixture was heated to 120 °C for 1 h with the protection of N_2, then the temperature was raised to 250 °C and kept for 5 min. After that, the mixture of 0.6 mL OAm–Cl and 0.4 mL OAm–Br was swiftly injected. Then, the obtained product was cooled to room temperature for further usage.

Purification: The $CsPbX_3$ and $Mn:CsPbX_3$ NCs were extracted from the crude solution by centrifuging at 6000 rpm for 5 min and the supernatants were discarded to remove unreacted precursor and by-products. The precipitate was redispersed in 1 mL toluene, then centrifuged at 10 000 rpm for 5 min. This step was repeated twice and the final precipitate was dissolved in 5 mL hexane for further usage.

Preparation of $Mn:CsPbX_3$ (X = Cl, Br) NC Powders: Purified $Mn:CsPbX_3$ (X = Cl, Br) NCs were dissolved in 5 mL toluene and dried in a vacuum freeze dryer for 12 h.

Construction of Perovskite NC–Based Light-Emitting Diode: The as-prepared $CsPbBr_3$ NCs and $Mn:CsPb(Cl_{0.6}Br_{0.4})_3$ NCs were spin-coated onto the glass slices (20 mm × 20 mm) to fabricate perovskite emitting layers. White light-emitting diode devices were constructed by coupling the $CsPbBr_3$ NC layer and $Mn:CsPb(Cl_{0.6}Br_{0.4})_3$ NC layers on the 365 nm UV chip. The edge of device was filled with opaque silica gels to avoid UV leakage of chip.

Characterizations: XRD analysis was carried out to identify perovskite phase structures using a powder diffractometer (MiniFlex600 RIGAKU) with Cu K_α radiation (λ = 0.154 nm) operating at 40 kV. Microstructure observations of Mn-doped $CsPbX_3$ perovskite NCs were carried out on a JEOL JEM-2010 TEM operated at 200 kV accelerating voltage equipped with an EDX spectroscopy system. Scanning transmission electron microscope (STEM) images and element mappings were recorded on a FEI aberration-corrected Titan Cubed S-Twin microscope operated on a HAADF mode. The actual chemical compositions were determined by ICP technique using a Perkin-Elmer Optima 3300DV spectrometer. Electron paramagnetic resonance (EPR) spectra were recorded by an E-580 Bruker Elexsys X-band EPR spectrometer. The optical absorption spectra were recorded by a spectrophotometer (Lambda900, Perkin-Elmer) with a resolution of 1 nm. PL spectra and Mn^{2+} decay curves were recorded on an Edinburgh Instruments FLS1000 spectrofluorometer equipped with 450 W xenon lamps and 60 W pulse xenon lamps as the excitation sources. Time-resolved spectra for exciton recombination were detected on a fluorescent lifetime spectrometer (Edinburgh Instruments, LifeSpec-II) based on a time correlated single photon counting technique under the excitation of 375 nm picosecond laser. PLQY, defined as the ratio of emitted photons to absorbed ones, was determined by a spectra fluorometer (FLS1000) equipped with the xenon lamp as the excitation source and a 15 cm integrating sphere. Temperature-dependent PL spectra were measured on an Edinburgh Instruments FLS980 spectrofluorometer equipped with a Linkam THMS600 temperature controlling stage. Electroluminescence spectra, Commission Internationale de L'Eclairage (CIE) chromaticity coordinates, color rendering index, correlated color temperature, and luminous efficiency for the designed lighting devices were recorded in a HAAS-2000 spectroradiometer (Everfine, HAAS-2000) at room temperature.

Supporting Information

Supporting Information is available from the Wiley Online Library or from the author.

Acknowledgements

D.Q.C. and S.Z. contributed equally to this work. This research was supported by the National Key Research and Development Program of China (Grant No. 2018YFB0406704), the National Natural Science Foundation of China (Grant No. 51572065), and the Fujian Normal University Training Program of Innovation and Entrepreneurship for Undergraduates (Grant No. cxxl-2019132).

Conflict of Interest

The authors declare no conflict of interest.

Keywords

doping, luminescence, optical materials, perovskites, white light-emitting diodes

Received: June 28, 2019
Revised: July 25, 2019
Published online:

[1] F. Zhang, H. Zhong, *ACS Nano* **2015**, *9*, 4533.
[2] Q. A. Akkerman, V. D'Innocenzo, S. Accornero, A. Scarpellini, A. Petrozza, M. Prato, L. Manna, *J. Am. Chem. Soc.* **2015**, *137*, 10276.
[3] X. S. Tang, W. W. Chen, Z. Z. Liu, J. Du, Z. Q. Yao, Y. Huang, C. Chen, Z. Q. Yang, T. C. Shi, W. Hu, Z. G. Zang, Y. Chen, Y. X. Leng, *Small* **2019**, *15*, 1900484.
[4] T. Chiba, Y. Hayashi, H. Ebe, K. Hoshi, J. Sato, S. Sato, Y. J. Pu, S. Ohisa, J. Kido, *Nat. Photonics* **2018**, *12*, 681.
[5] Y. Fu, H. Zhu, A. W. Schrader, D. Liang, Q. Ding, P. Joshi, L. Hwang, X. Y. Zhu, S. Jin, *Nano Lett.* **2016**, *16*, 1000.
[6] J. Li, L. Xu, T. Wang, J. Song, J. Chen, J. Xue, Y. Dong, B. Cai, Q. Shan, B. Han, H. Zeng, *Adv. Mater.* **2017**, *29*, 1603885.
[7] X. Li, Y. Wu, S. Zhang, B. Cai, Y. Gu, J. Song, H. Zeng, *Adv. Funct. Mater.* **2016**, *26*, 2435.
[8] K. Lin, J. Xing, L. N. Quan, F. P. G. de Arquer, X. Gong, J. Lu, L. Xie, W. Zhao, D. Zhang, C. Yan, W. Li, X. Liu, Y. Lu, J. Kirman, E. H. Sargent, Q. Xiong, Z. Wei, *Nature* **2018**, *562*, 245.
[9] Z. Liu, J. Yang, J. Du, Z. Hu, T. Shi, Z. Zhang, Y. Liu, X. Tang, Y. Leng, R. Li, *ACS Nano* **2018**, *12*, 5923.
[10] L. Protesescu, S. Yakunin, M. I. Bodnarchuk, F. Krieg, R. Caputo, C. H. Hendon, R. X. Yang, A. Walsh, M. V. Kovalenko, *Nano Lett.* **2015**, *15*, 3692.
[11] J. Song, J. Li, X. Li, L. Xu, Y. Dong, H. Zeng, *Adv. Mater.* **2015**, *27*, 7162.
[12] T. Debnath, H. N. Ghosh, *J. Phys. Chem. C* **2019**, *123*, 10703.
[13] S. Mahamuni, A. D. Lad, S. Patole, *J. Phys. Chem. C* **2008**, *112*, 2271.
[14] R. Beaulac, P. I. Archer, S. T. Ochsenbein, D. R. Gamelin, *Adv. Funct. Mater.* **2008**, *18*, 3873.
[15] V. A. Vlaskin, N. Janssen, J. van Rijssel, R. Beaulac, D. R. Gamelin, *Nano Lett.* **2010**, *10*, 3670.
[16] D. Parobek, B. J. Roman, Y. Dong, H. Jin, E. Lee, M. Sheldon, D. H. Son, *Nano Lett.* **2016**, *16*, 7376.
[17] A. K. Guria, S. K. Dutta, S. Das Adhikari, N. Pradhan, *ACS Energy Lett.* **2017**, *2*, 1014.
[18] W. Liu, Q. Lin, H. Li, K. Wu, I. Robel, J. M. Pietryga, V. I. Klimov, *J. Am. Chem. Soc.* **2016**, *138*, 14954.
[19] W. J. Mir, Y. Mahor, A. Lohar, M. Jagadeeswararao, S. Das, S. Mahamuni, A. Nag, *Chem. Mater.* **2018**, *30*, 8170.
[20] K. Xu, A. Meijerink, *Chem. Mater.* **2018**, *30*, 5346.
[21] P. Arunkumar, K. H. Gil, S. Won, S. Unithrattil, Y. H. Kim, H. J. Kim, W. B. Im, *J. Phys. Chem. Lett.* **2017**, *8*, 4161.
[22] J. Zhu, X. Yang, Y. Zhu, Y. Wang, J. Cai, J. Shen, L. Sun, C. Li, *J. Phys. Chem. Lett.* **2017**, *8*, 4167.
[23] S. Hou, M. K. Gangishetty, Q. Quan, D. N. Congreve, *Joule* **2018**, *2*, 2421.
[24] F. Li, Z. Xia, C. Pan, Y. Gong, L. Gu, Q. Liu, J. Z. Zhang, *ACS Appl. Mater. Interfaces* **2018**, *10*, 11739.
[25] H. Liu, Z. Wu, J. Shao, D. Yao, H. Gao, Y. Liu, W. Yu, H. Zhang, B. Yang, *ACS Nano* **2017**, *11*, 2239.
[26] W. J. Mir, M. Jagadeeswararao, S. Das, A. Nag, *ACS Energy Lett.* **2017**, *2*, 537.
[27] S. Zou, Y. Liu, J. Li, C. Liu, R. Feng, F. Jiang, Y. Li, J. Song, H. Zeng, M. Hong, X. Chen, *J. Am. Chem. Soc.* **2017**, *139*, 11443.
[28] S. Das Adhikari, S. K. Dutta, A. Dutta, A. K. Guria, N. Pradhan, *Angew. Chem., Int. Ed.* **2017**, *56*, 8746.
[29] A. Dutta, R. K. Behera, P. Pal, S. Baitalik, N. Pradhan, *Angew. Chem., Int. Ed.* **2019**, *58*, 5552.
[30] Y. Wu, C. Wei, X. Li, Y. Li, S. Qiu, W. Shen, B. Cai, Z. Sun, D. Yang, Z. Deng, H. Zeng, *ACS Energy Lett.* **2018**, *3*, 2030.
[31] Z. J. Yong, S. Q. Guo, J. P. Ma, J. Y. Zhang, Z. Y. Li, Y. M. Chen, B. B. Zhang, Y. Zhou, J. Shu, J. L. Gu, L. R. Zheng, O. M. Bakr, H. T. Sun, *J. Am. Chem. Soc.* **2018**, *140*, 9942.
[32] D. Yang, X. Li, Y. Wu, C. Wei, Z. Qin, C. Zhang, Z. Sun, Y. Li, Y. Wang, H. Zeng, *Adv. Opt. Mater.* **2019**, *7*, 1900276.
[33] X. Yuan, S. Ji, M. C. De Siena, L. Fei, Z. Zhao, Y. Wang, H. Li, J. Zhao, D. R. Gamelin, *Chem. Mater.* **2017**, *29*, 8003.
[34] D. Chen, G. Fang, X. Chen, L. Lei, J. Zhong, Q. Mao, S. Zhou, J. Li, *J. Mater. Chem. C* **2018**, *6*, 8990.
[35] D. Chen, S. Zhou, G. Fang, X. Chen, J. Zhong, *ACS Appl. Mater. Interfaces* **2018**, *10*, 39872.
[36] D. Chen, X. Chen, *J. Mater. Chem. C* **2019**, *7*, 1413.
[37] G. Huang, C. Wang, S. Xu, S. Zong, J. Lu, Z. Wang, C. Lu, Y. Cui, *Adv. Mater.* **2017**, *29*, 1700095.
[38] Q. A. Akkerman, D. Meggiolaro, Z. Dang, F. De Angelis, L. Manna, *ACS Energy Lett.* **2017**, *2*, 2183.